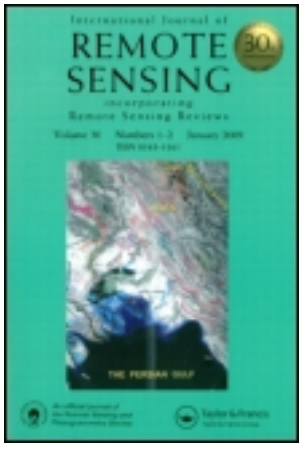

International Journal of Remote Sensing

Publication details, including instructions for authors and subscription information:
http://www.tandfonline.com/loi/tres20

Thermal imaging of Nisyros volcano (Aegean Sea) using ASTER data: estimation of radiative heat flux

A. Ganas [a] , E. Lagios [b] , G. Petropoulos [c] & B. Psiloglou [d]

[a] Geodynamics Institute, National Observatory of Athens, PO Box 20048, Athens, 118 10, Greece

[b] Space Applications Unit in Geosciences, Department of Geophysics & Geothermics, University of Athens, Panepistimiopolis - Ilissia, Athens, 157 84, Greece

[c] Department of Geography, King's College London, Strand Campus, WC2R 2LS, London, UK

[d] Institute of Environmental Research and Sustainable Development, National Observatory of Athens, I. Metaxa & Vas. Pavlou Str., 152 36, Athens, Greece

Available online: 13 Sep 2010

To cite this article: A. Ganas, E. Lagios, G. Petropoulos & B. Psiloglou (2010): Thermal imaging of Nisyros volcano (Aegean Sea) using ASTER data: estimation of radiative heat flux, International Journal of Remote Sensing, 31:15, 4033-4047

To link to this article: http://dx.doi.org/10.1080/01431160903140837

International Journal of Remote Sensing
Vol. 31, No. 15, 10 August 2010, 4033–4047

Taylor & Francis
Taylor & Francis Group

Thermal imaging of Nisyros volcano (Aegean Sea) using ASTER data: estimation of radiative heat flux

A. GANAS*†, E. LAGIOS‡, G. PETROPOULOS**§ and B. PSILOGLOU¶
†Geodynamics Institute, National Observatory of Athens, PO Box 20048, Athens 118 10, Greece
‡Space Applications Unit in Geosciences, Department of Geophysics & Geothermics, University of Athens, Panepistimiopolis – Ilissia, Athens 157 84, Greece
§Department of Geography, King's College London, Strand Campus, WC2R 2LS, London, UK
¶Institute of Environmental Research and Sustainable Development, National Observatory of Athens, I. Metaxa & Vas. Pavlou Str., 152 36 Athens, Greece

(*Received 15 March 2008; in final form 23 September 2008*)

A time series of Advanced Spaceborne Thermal Emission and Reflection Radiometer (ASTER) images (AST08) have been processed to allow radiative heat flux estimations of the Nisyros volcano. ASTER night-time images were acquired on four different dates: 7 April 2001, 13 June 2002, 26 October 2002 and 23 July 2005. The results show a steady state energy release with heat fluxes ranging from 15 to 30 W m^{-2} over the craters of Kaminakia, Polyvotis and Stefanos, respectively. It is suggested that this range of values indicates a background heat flux of this volcano following the unrest of 1995–1997, and that the volcano has entered again into the quiet phase. Also, on the basis of the average spatial extent of the thermal anomaly a total radiative heat flux of 36 MW was estimated at the moment of ASTER overpass. Heat flux values for Nisyros are in good agreement with other published estimates derived from low-temperature fumarolic volcanoes (Stromboli and Vulcano, Italy) using Landsat TM data. It is also evidenced that the ASTER radiometer can be used as an important imaging tool for the monitoring of geophysical properties associated to volcanic activity, as is the volcanic heat flux.

1. Introduction

1.1 *The Nisyros setting*

Nisyros is an active strato-volcano in the Aegean Sea (Greece; 36° 30′ N, 27° 15′ E; figure 1) of mainly andesitic-rhyolitic composition (Vougioukalakis 1993) and about 7 km diameter in size. The volcano has recently gained attention from the geosciences community because of its renewed activity during 1995–1997 (Papadopoulos *et al.* 1998, Lagios *et al.* 2007). This crisis did not trigger any hydrothermal eruption but was followed by important variations both in the chemistry of fumarolic gases

*Corresponding author. Email: aganas@gein.noa.gr
**Now at: Department of Earth Sciences, University of Bristol, Wills Memorial Building, Queens Road, Bristol, BS8 1RJ,UK

International Journal of Remote Sensing
ISSN 0143-1161 print/ISSN 1366-5901 online
http://www.tandf.co.uk/journals
DOI: 10.1080/01431160903140837

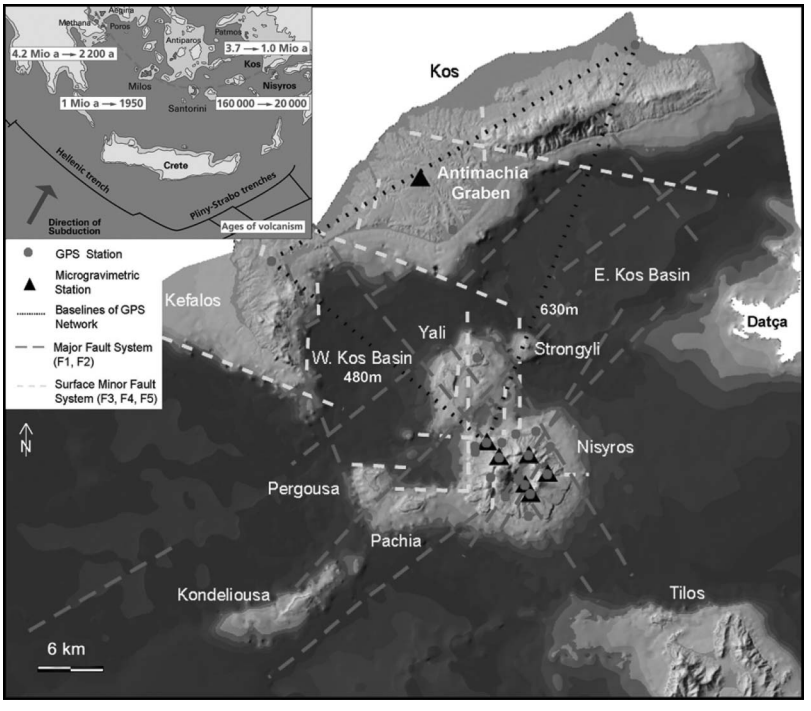

Figure 1. Setting of the Nisyros volcano in the south-east Aegean Sea. Inset box shows the location of the Quaternary volcanoes of the Aegean Arc and ages of volcanism. Image from the GEOWARN website (Gogu *et al*. 2006): http://www.geowarn.ethz.ch. Details of geophysical instrumentation are reported in Lagios *et al*. (2005).

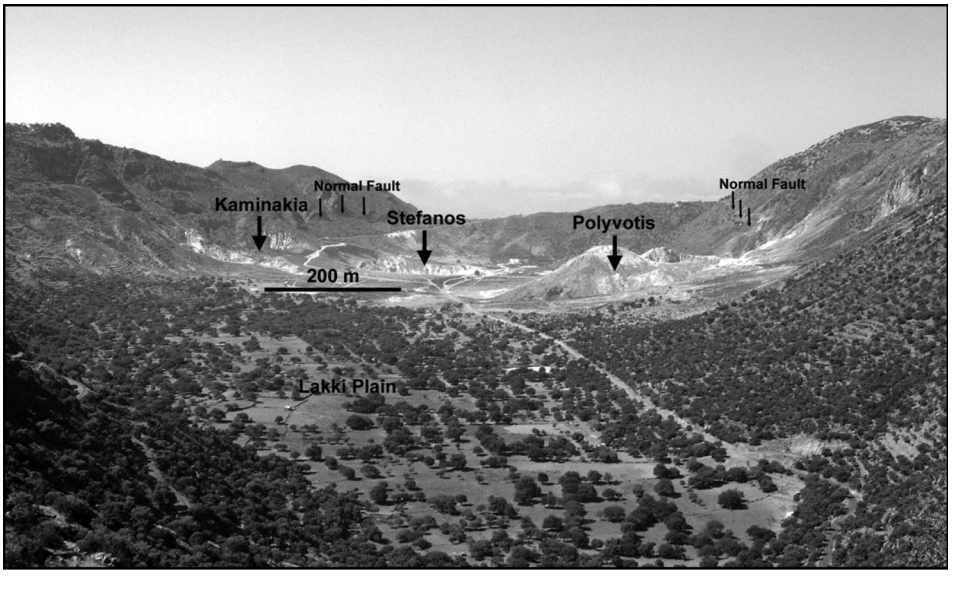

Figure 2. Field photograph of the Nisyros caldera (20 May 2002). View to the south. The crater areas are shown by thick black arrows. Thin black arrows point to normal faults that dip towards the interior of the caldera. Photograph by AG.

(Chiodini *et al.* 2002) and in surface deformation (Sachpazi *et al.* 2002, Sykioti *et al.* 2003, Lagios *et al.* 2005). Today, the area of the hydrothermal craters (Polyvotis, Stefanos and Kaminakia; figure 2) of the summit caldera (Lakki Plain) is affected by an intense activity of fumaroles, hot soils and diffuse degassing of CO_2 (Caliro *et al.* 2005, Teschner *et al.* 2007).

Fumaroles are vents from which volcanic gases escape into the atmosphere. In Nisyros the fumaroles occur mainly inside the hydrothermal craters (figure 2) along tiny, centimetre-size cracks, metre-size fissures, and in small clusters. They occur at altitudes between 90 and 130 m. They persist for centuries as they are above a persistent heat source (active magma chamber; Georgalas (1962), Marini *et al.* (1993)). All the fumaroles have outlet temperatures close to the boiling point of water (96–100°C; Chiodini *et al.* (2002), Teschner *et al.* (2007)). Their activity is also linked to active normal faults striking NE–SW and N–S (Marini *et al.* 1993, Caliro *et al.* 2005; figure 2). The craters hosting the fumaroles are formed on caldera sediments and detritus.

This paper uses Advanced Spaceborne Thermal Emission and Reflection Radiometer (ASTER) data from night-time passes taken over Nisyros island and seeks: (a) to demonstrate the use of ASTER thermal infrared data in monitoring low-temperature volcanoes, such as the one in the Nisyros setting; (b) to present proof of the sensor capability for mapping hydrothermal activity inside calderas; and (c) to provide estimates of radiative heat flux above fumarolic fields on Nisyros. Monitoring this particular volcano from space is important as Nisyros is one of the two Greek volcanoes currently active, with the last episode of unrest taking place in 1995–1997. Night-time observations were used to minimize the effect of surficial solar heating so as to allow better delineation of low-temperature geothermal anomalies in thermal infrared (TIR) bands. Furthermore, the saturation temperature in the TIR (8–12 μm) is 97.0°C (Pieri and Abrams 2004) while previous studies (e.g. Ganas and Lagios 2003, Ganas *et al.* 2003, Lagios *et al.* 2007) have shown that night-time whole-pixel temperatures inside the Nisyros caldera range from 13.0 to 28.0°C. Four ASTER surface kinetic temperature scenes (AST08—higher level product) were processed to estimate radiative heat flux from the crater region of Nisyros. The image analysis followed the methodology of Gaonac'h *et al.* (1994) and Harris and Stevenson (1997). Results from this study constitute the first time-series heat flux data for this volcano.

1.2 *The ASTER sensor*

ASTER (Advanced Spaceborne Thermal Emission and Reflection Radiometer) is a joint Japanese–NASA multispectral sensor carried on the TERRA satellite, which was launched on 18 December 1999. Data formats and applications are discussed among others by Abrams and Hook (1999), Yamaguchi *et al.* (1999) and Fujisada *et al.* (1998). A brief summary of the sensor's technical specifications is shown in table 1. Briefly, ASTER is a narrow field-of-view sensor (the swath angle of the sensor is $\pm$ 2.4°), which scans a swath of 60 km on the ground. The sensor has nine reflective bands in the visible and near-infrared (VNIR) and shortwave infrared (SWIR) and five bands in the TIR. In particular, the acquisition of imaging data in five spectral channels in the TIR allows better temperature and thermal emissivity separation than has been previously possible. The presence of five bands makes it possible to identify wavelength-dependent variations in emissivity so that true kinetic temperatures can be estimated. In addition, ASTER has 12-bit quantization, a radiometric precision (NEΔT; noise equivalent

Table 1. Characteristics of the ASTER sensor (after Fujisada *et al*. 1998, Abrams and Hook 1999, Yamaguchi *et al*. 1999).

Characteristic	VNIR	SWIR	TIR
Spectral range	• Band 1: 0.52–0.60 μm (nadir looking) • Band 2: 0.63–0.69 μm (nadir looking) • Band 3N: 0.76–0.86 μm (nadir looking) • Band 3B: 0.76–0.86 μm (backward looking)	• Band 4: 1.600–1.700 μm • Band 5: 2.145–2.185 μm • Band 6: 2.185–2.225 μm • Band 7: 2.235–2.285 μm • Band 8: 2.295–2.365 μm • Band 9: 2.360–2.430 μm	• Band 10: 8.125–8.475 μm • Band 11: 8.475–8.825 μm • Band 12: 8.925–9.275 μm • Band 13: 10.25–10.95 μm • Band 14: 10.95–11.65 μm
Ground resolution (m)	15	30	90
1-σ calibration uncertainty	$\leq \pm 4\%$	$\leq \pm 4\%$	Band 10: ≤ 3 K (200–240 K) Bank 11: ≤ 2 K (240–270 K) Band 12: ≤ 1 K (270–340 K) Band 13: ≤ 2 K (340–370 K)
Cross-track pointing	$\pm 24^\circ$	$\pm 8.55^\circ$	$\pm 8.55^\circ$
Quantization levels	8 bits	8 bits	12 bits
Swath width (km)	60	60	60
Orbit	Sun-synchronous, descending		
Altitude range	700–737 km (705 km at the equator)		
Inclination	$98.2^\circ \pm 0.15'$		
Repeat cycle	16 days (233 revolutions / 16 days)		
Orbit period	98.9 min		
Stereo base / height ratio	0.6 (along-track)		

delta temperature) of 0.3 K, and one standard deviation calibration uncertainty of 1.0 K between 270.0 and 340.0 K. In this respect, ASTER is superior to Landsat because of (a) its 12-bit quantization in the thermal infrared channels and (b) more accurate surface temperature estimate because the AST08 product (kinetic temperature) uses the Temperature Emissivity Separation (TES) algorithm (Gillespie *et al.* 1998) on five thermal channels.

The use of ASTER thermal data in the detection of thermal anomalies above several volcanoes around the planet has been previously demonstrated in many studies (Ramsey and Dehn 2004, Pieri and Abrams 2004, 2005, Vaughan and Hook 2006) including geothermal activity areas (Coolbaugh *et al.* 2007). On Nisyros island, previous work has shown that the whole-pixel temperature map extracted from ASTER band-13 night-time data is reasonably accurate and in agreement with Landsat 7 ETM+ results (Ganas and Lagios 2003, Ganas *et al.* 2003), retrieving surface temperatures in the range 13.0–28.0°C. On the other hand, for volcanoes with high surface temperatures above 150.0°C, short-wavelength infrared (SWIR) bands 5 (1.55–1.75 μm) and 7 (2.08–2.35 μm) of the Landsat Thematic Mapper (TM) have successfully been used (Rothery *et al.* 1988, Oppenheimer 1991).

2. Data processing

Heat flux is the energy flowing through a surface of 1 m^2 in one second and is a vector quantity measured in W m^{-2}. In this work, radiative heat flux (Q_{rel}) in Nisyros was derived using four cloud-free night-time ASTER images acquired over the area of interest on 7 April 2001, 13 June 2002, 26 October 2002 and 23 July 2005. The night-time images contain many pixels with low digital values and no stripping effects (7 April 2001 and 26 October 2002) or some stripping (13 June 2002 and 23 July 2005). No attempt was made to filter those effects from the imagery, as this would effectively degrade image quality in areas where the effects were less evident. Low-value pixels were found most abundantly (a) outside of the caldera (the western part of the image at high elevations; figure 3); and (b) along the eastern, inner slope of the caldera

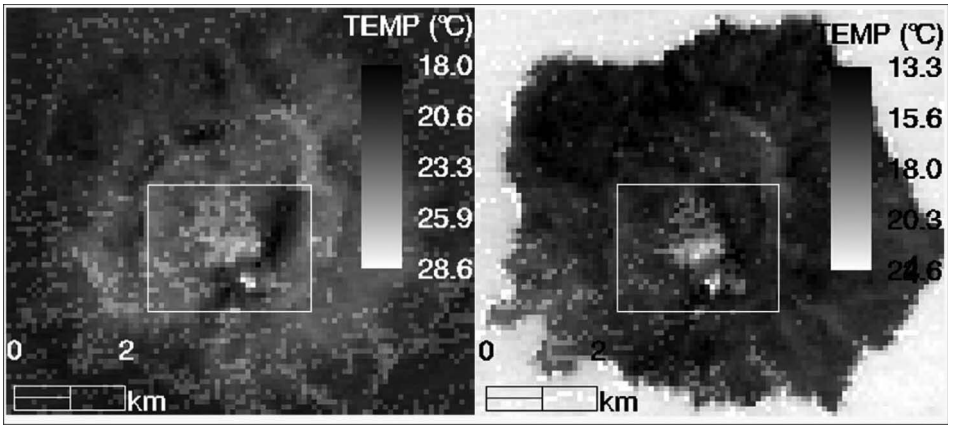

Figure 3. Temperature map of the Nisyros volcano after applying equation (1). Increasing brightness indicates warmer surface temperatures. The map shows values of θ for 13 June 2002 (left) and 26 October 2002 (right), respectively. White box indicates location of craters and extent of figure 4.

(figures 2 and 3). All image processing was done in ENVI desktop platform. AST08 images were provided from Earth Remote Sensing Data Analysis Center (ERSDAC) Ground Data System (GDS) Information Management Service (IMS). They were initially geometrically corrected using the information embedded in the images header files, following the procedure outlined in the ASTER User's Handbook (Abrams and Hook 1999). The procedure comprises of the following: (a) specifying the values for the corner column-row (pixel-line) image coordinates; (b) specifying the correct pixel resolution for the x and y directions; (c) specifying the map orientation angle value; and (d) indicating the output projection coefficients including the projection, zone and datum. After implementation of this procedure, geo-positional accuracy is expected to be in the order of the sensor pixel size (here 90 m) in the x and y directions (ASTER Science Project User's Guide 2005). Subsequently, improvement of the geo-positional accuracy was done using image-to-vector georeferencing using a high-resolution coastline from 1:5000 maps of the Greek Army and performing 1st polynomial transformations. The correction was difficult because of the night acquisition, and only seven control points could be matched with the 7 April 2001 (master) image. The registration error for this image was improved to approximately 45 m. The remaining three AST08 images as well as the four AST05 images were registered to the master image with comparable error (0.5 pixels). Image resampling was done using the nearest neighbour technique to preserve original temperatures.

The image analysis considers whole-pixel kinetic temperatures, while it is well-known that the Nisyros craters are characterized by active volcanic vents, fumaroles and fractures (Marini *et al.* 1993, Chiodini *et al.* 2002). At 10-cm depth, soil temperatures inside the Stefanos crater (see figure 2 for location) could reach 58.0°C (Ganas and Lagios 2003, Lagios *et al.* 2007) but this distribution of temperatures is heterogeneous and changes with time. Based on previous fieldwork conducted in Nisyros, it is estimated that fumaroles and other heat sources on Nisyros are 2–3 orders of magnitude smaller than the ASTER pixel size (8100 m^2) and their temperatures do not exceed 100.0°C. This in fact means that such heat sources provide only a small contribution to the integrated pixel temperature of ASTER (25.0–28.6°C; figure 4) and thus can be neglected for the purposes of this study. Nevertheless, the total heat

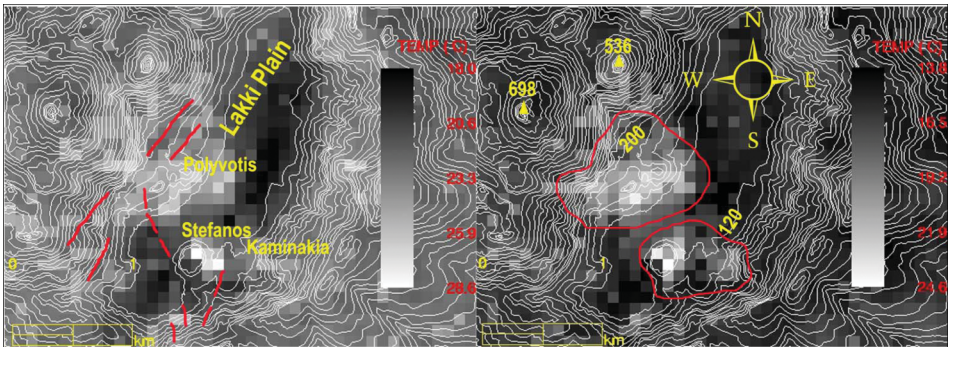

Figure 4. Temperature map of the crater region inside the Nisyros caldera on 13 June 2002 (left) and 26 October 2002 (right). Thin white lines are elevation contours (interval 20 m). Red lines on the left image indicate normal faults, after http://www.geowarn.ethz.ch/images/screenshots/layers_geology_zoom_large.jpg. Red polygons on the right image indicate extent of thermal anomalies used to calculate total flux in the Nisyros caldera.

flux is a bit higher that the calculated discharge by the above method because of the averaging effect of the ASTER pixel (0.81 ha).

Assuming an isothermal pixel structure for the thermal anomaly and following Gaonac'h *et al.* (1994) and Harris and Stevenson (1997), heat flux (Q_{rel}) was calculated using the kinetic temperature obtained from the AST08 higher level product, and the emissivity supplied as a separate product by the TES algorithm (Gillespie *et al.* 1998). In brief, the TES algorithm relies on an empirical relationship between spectral contrast and minimum emissivity, determined from laboratory and field emissivity spectra to equalize the number of unknowns and measurements so that the set of Planck equations for the measured thermal radiances can be inverted. In the TES algorithm, the additional constraint comes from the regression of minimum emissivity to spectral contrast calculated from laboratory spectra. According to Gaonac'h *et al.* (1994) the accuracy of Q_{rel} estimate (equation (2) below) is up to 19% of the mean value using Landsat 5 TM data for the Stromboli region, while Harris and Stevenson (1997) reevaluated the accuracy of equation (2) for the Vulcano region as within 5% of the mean value.

In detail, a height-independent, corrected temperature (θ) was calculated for each pixel in order to remove surface temperature variations caused by cooler air temperatures at higher altitudes (Bonneville *et al.* (1985); in Nisyros this was detected on Landsat imagery by Ganas and Lagios (2003)):

$$\theta = T + h\alpha, \tag{1}$$

where T is the ASTER-derived surface temperature (product AST08), h is surface altitude and α is the adiabatic gradient (0.006°C m^{-1}). Then Q_{rel} is:

$$Q_{rel} = 4.614\varepsilon[0.52 + 0.065(e)^{0.5}]\Delta\theta, \tag{2}$$

where e is vapour pressure (mbar) and $\Delta\theta$ is the difference in °C between maximum θ within the thermal anomaly (crater) and minimum θ from all pixels near to the anomaly (Gaonac'h *et al.* (1994); table 2). Note that the AST08 product had been preprocessed to convert radiance temperatures to kinetic temperatures using the algorithms of Gillespie *et al*. (1998).

The temperature difference was determined by georeferencing the AST08 scene to a 20-m digital elevation model (DEM) of the volcano and applying image algebra using equation (2) (figure 3). The AST08 product delivers scaled kinetic temperature values which were first converted to Kelvin and then to °C. Then θ values were extracted from the final image product for all dates. For example, during the 13 June 2002 overpass the maximum temperature inside the Stefanos crater (figure 4) was found to be 28.6°C and the minimum temperature outside the thermal anomaly was 18.4°C, so computed $\Delta\theta$ was 8.2°C (table 2). Also, the October 2002 range of caldera temperatures (13.8–24.6°C; figure 4) is in close agreement with previous work by Ganas and Lagios (2003) with Landsat ETM+ night-scene data (20 October 2000 overpass) where they showed that the temperature variability in Nisyros was 13.0–22.0°C and the accuracy against ground data was 0.4–2.0°C.

For determining spectral emissivity (ε) of the crater surface the maximum value from the AST05 product was used in all five bands. The vapour pressure (e) for each date was calculated from the radiosonde data of the Heraklion Airport in Northern Crete which are available on the Internet on a daily basis (http://weather.uwyo.edu/upperair/sounding.html). The altitude of the calculation was between 100 and 120 m,

Table 2. Results of the radiative heat flux calculations. Θ_{max}–Θ_{min} is temperature difference $\Delta\theta$ in equation (2), vapour pressure is in mbar and Q_{rel} in W m^{-2}. The UTM coordinates of pixels with calculated Θ_{max} and Θ_{min} are shown as E (east) and N (north), respectively. The mean surface temperature Θ and standard deviation for each acquisition time is the following: 7 April 2001 20:23 UTC (12.49°C; 2.82°C), 13 June 2002 20:15 UTC (20.27°C; 1.11°C), 26 October 2002 20:20 UTC (17.06°C; 3.47°C) and 23 July 2005 20:12 UTC (23.32°C; 1.3°C). Local time is UTC + 3:00 h.

Date	Crater	Θ_{max} (°C)	Θ_{min} (°C)	$\Delta\Theta$	Pixel Θ_{max}	Pixel Θ_{min}	AST05 spectral emissivity (band 13)	Vapour pressure (mbar)	Q_{rel}
7 April 2001	Stefanos	19.4	9.4	10.0	51° 49′ 62″ E–40° 47′ 995″ N	51° 48′ 72″ E–40° 47′ 905″ N	0.964	11.36	32.874
13 June 2002	Stefanos	28.6	18.4	8.2	51° 50′ 52″ E–40° 48′ 175″ N	51° 47′ 82″ E–40° 47′ 995″ N	0.962	16.73	28.603
26 October 2002	Stefanos	23.2	14.2	9.0	51° 50′ 52″ E–40° 48′ 085″ N	51° 48′ 72″ E–40° 47′ 995″ N	0.964	17.14	31.589
23 July 2005	Stefanos	32.4	23.4	9.0	51° 50′ 52″ E–40° 48′ 085″ N	51° 46′ 92″ E–40° 47′ 905″ N	0.964	19.87	32.415
7 April 2001	Polyvotis	16.6	8.3	8.3	51° 46′ 92″ E–40° 48′ 625″ N	51° 52′ 32″ E–40° 48′ 625″ N	0.964	11.36	27.285
13 June 2002	Polyvotis	26.8	18.1	8.7	51° 50′ 52″ E–40° 48′ 805″ N	51° 55′ 92″ E–40° 48′ 805″ N	0.964	16.73	30.410
26 October 2002	Polyvotis	21.9	13.8	8.1	51° 47′ 82″ E–40° 48′ 625″ N	51° 53′ 22″ E–40° 48′ 625″ N	0.965	17.14	28.459
23 July 2005	Polyvotis	30.4	23.4	7.0	51° 46′ 92″ E–40° 48′ 535″ N	51° 53′ 22″ E–40° 48′ 625″ N	0.964	19.87	25.212
7 April 2001	Kaminakia	13.5	9.5	4.0	51° 55′ 02″ E–40° 48′ 085″ N	51° 53′ 22″ E–40° 47′ 905″ N	0.964	11.36	13.149
13 June 2002	Kaminakia	25.3	18.3	7.0	51° 55′ 92″ E–40° 48′ 085″ N	51° 53′ 22″ E–40° 48′ 445″ N	0.967	16.73	24.544
26 October 2002	Kaminakia	18.6	13.8	4.8	51° 55′ 92″ E–40° 48′ 085″ N	51° 53′ 22″ E–40° 48′ 625″ N	0.966	17.14	16.882
23 July 2005	Kaminakia	27.8	23.4	4.4	51° 55′ 92″ E–40° 48′ 175″ N	51° 53′ 22″ E–40° 48′ 625″ N	0.964	19.87	15.847

Table 3. Surface meteorological data measured at Kos Airport (elevation 115 m) during each satellite overpass. The airport is located approximately 25 km to the north of Nisyros caldera (see figure 1 for location). EEST is East European Summer Time (UTC + 3:00). Dew point is the temperature to which air must be cooled, at constant barometric pressure, for water vapour to condense into water. e is actual vapour pressure (in mbar) calculated according to Hyland and Wexler (1983).

Date	Time (EEST)	Air temperature (°C)	Dew point temperature (°C)	Relative humidity (%)	Pressure at sea level (hPa)	Wind speed (km h^{-1})	e
7 April 2001	11:20 pm	16	10	68	1014	4.6	12.27
13 June 2002	10:20 pm	23	18	73	1010	6.9	20.61
26 October 2002	11:20 pm	16	11	72	1017	4.6	13.11
23 July 2005	11:20 pm	23	19	78	1009	8.1	21.94

which is the average elevation of the Nisyros caldera. To calculate vapour pressure the method of Hyland and Wexler (1983) was employed. The radiosonde-based values were compared against vapour pressure values derived from surface meteorological data from the Kos airport, which is located about 25 km to the north of the Nisyros caldera (figure 1; table 3). A good agreement was found for all dates except for the 26 October 2002 overpass where our radiosonde value is about 30% higher than the Kos airport one. This difference is expected to provide higher Q_{rel} numbers for this particular date but it has a negligible effect on the observed Q_{rel} patterns, as shown later. After solving equation (2) Q_{rel} is computed for each thermal anomaly distributed across 8100 m^2, which is the pixel area of the TIR sensor.

3. Discussion

3.1 *Heat flux pattern and amounts*

The results from the analysis are presented in figures 5, 6 and 7 and in table 2. To examine the heat flux variation of Nisyros over time, a time series graph for each crater was constructed (figure 5). As can be observed, the Stefanos crater radiates more heat flux in comparison to the Polyvotis crater to the north-west. In addition, analysis of the results clearly suggests an almost steady state of heat flux over the period 2001–2005. This is an important geophysical observation as it essentially confirms the Interferometric Synthetic Aperture Radar (InSAR)-based findings (Sykioti *et al.* 2003) that the volcano has re-entered a phase of quiescence after the crisis of 1995–1997. Another interesting observation is that the Kaminakia crater radiates heat flux of approximately half the amount of the other two craters. Following figure 5 an average value of 30 W m^{-2} ($\pm$ 15%; see Gaonac'h *et al.* 1994 for discussion on error margin) is considered for the thermal anomalies in the Lakki plain (figure 4; 1 200 000 m^2). This way, a total value of 36 MW ($\pm$ 6 MW) of radiative heat flux is obtained inside the caldera. This result is indicative of the low level of the thermal anomaly of this volcano. The computed Q_{rel} value per m^2 is comparable to the results of Gaonac'h *et al.* (1994) for the Stromboli (29 W m^{-2}) and Vulcano (37 W m^{-2}) thermal anomalies detected on Landsat TM night imagery.

Furthermore, Caliro *et al.* (2005) estimate the amount of total thermal energy as 43 MW for the whole Lakki plain (see figure 2 for location) using geochemical surveys during the period 1999–2001, which is when the ASTER-based remote sensing

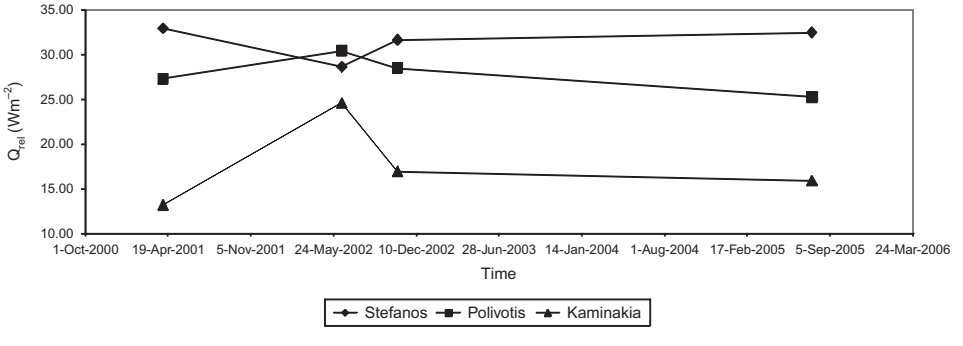

Figure 5. Diagram of radiative heat flux (Q_{rel}) measurement from ASTER data for Nisyros volcano over the period 2001–2005 (data from table 2).

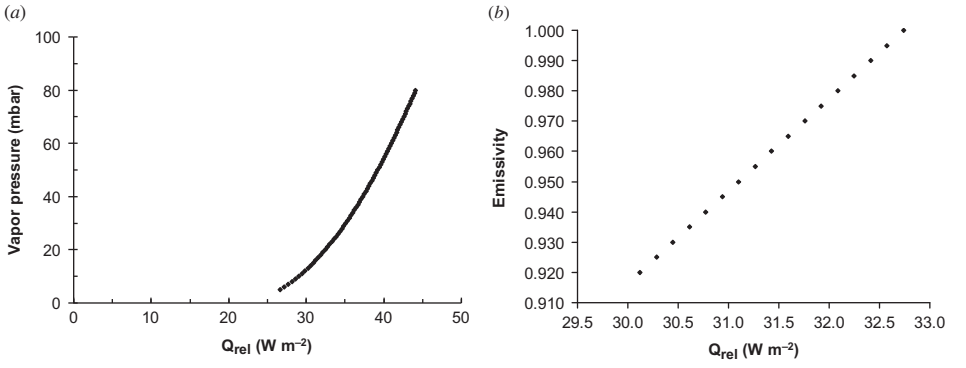

Figure 6. Diagrams showing nonlinear versus linear dependence of radiative heat flux (Q_{rel}) on vapour pressure (*a*) and spectral emissivity (*b*). Spectral emissivity of a material is the ratio of the spectral exitance of a material to the spectral exitance of a black body at the same temperature. Q_{rel} estimates refer to the October 2002 ASTER image (see table 2 for data).

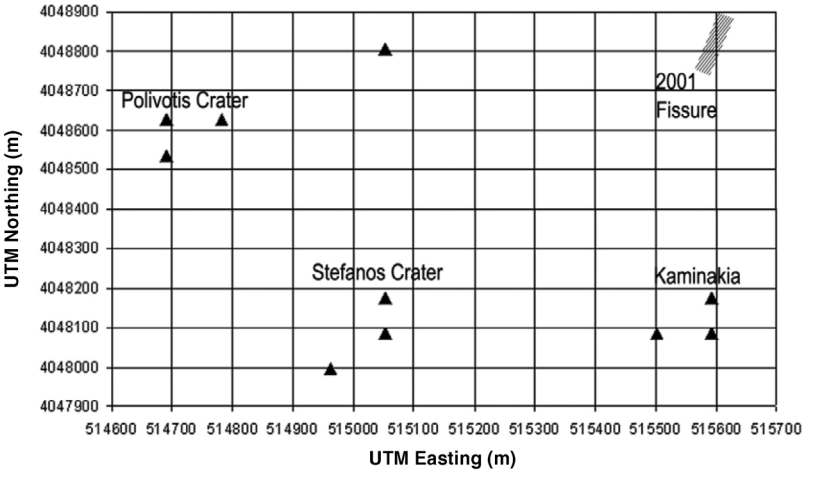

Figure 7. UTM grid showing the location of hot pixels for all four ASTER images. All hot spots are grouped in three areas except for the outlier in the Polyvotis region (13 June 2002). Double line with dots indicates location of fissure. Pixel size is 100 m.

estimates started. Their value is close to the ASTER-based estimates as a radiative heat flux of 36 MW was calculated for the same region with no change over a period of four years.

3.2 *Background heat flux and error analysis*

The analysis presented in this work has established the 'background' level of heat flux at about 36 MW for this volcano. The period of our observation (2001–2005) follows the latest unrest (peak in 1997), so it is reasonable to assume that this value is the 'background' reference. Other workers (Sykioti *et al.* 2003) have also showed that the volcano has entered the deflation phase after mid-1998, and no deformation was detected after 2000.

Further analysis explored the sensitivity of Q_{rel} to both water vapour and spectral emissivity, depicted in figure 6. The graph clearly manifests the nonlinear dependence of Q_{rel} on vapour pressure as opposed to its linear dependence on emissivity. In the former relationship Q_{rel} changes by over 30% when vapour pressure in the atmosphere increases from 20 to 60 mbar. Notably, Q_{rel} changes by 10% when emissivity of the surface increases from 0.92 to 0.99. This is another important observation as this highlights the nonlinear dependence of Q_{rel} on water vapour and it also highlights the need for radiosonde data closer to the volcano that would provide more accurate results.

To examine the impact of the input (remotely-sensed; AST08) temperature data on the Q_{rel} estimates, 1.0°C was added to the temperature data ($\Delta\theta$) of 26 October 2002. The calculations were then repeated again using equation (2). The new Q_{rel} estimate differs by an amount of 11% to the one in table 2, which is considered as acceptable error for regular heat flux monitoring of low-temperature volcanoes. Estimates of about 100% higher than the background are necessary to characterize a different phase in the volcanic cycle (Harris and Stevenson 1997).

3.3 *Hydrothermal system stability*

Figure 7 presents a map showing the 'hot-spots' inside the caldera, clearly pointing out the location of the hottest pixels in the caldera. It is assumed that the hottest pixels are associated with the position of the most active fumaroles inside the Nisyros caldera. Given the small error in image co-registration, results show an almost identical x–y location of hot-spots (in UTM coordinates) for all image acquisitions. Moreover, the spatial extent of the hottest areas is approximately 200 × 200 m (or 4 pixels; figure 7; x axis is east–west, y-axis is north–south), thus defining three areas (clusters) which correspond to the locations of major craters, i.e. Stefanos, Polyvotis and Kaminakia. This small movement of hot-spots (less than 200 m during 4 years) indicates an overall stability of the hydrothermal system of Nisyros for the period 2001–2005. There is one exception in the Polyvotis area (13 June 2002 overpass) where the 'hot-spot' pixel is about 350 m to the north-east of the cluster. The location of the pixel is about 500 m to the west of the termination of an extensional fissure that was created inside the flat caldera floor during December 2001 and became inactive during December 2002. The fissure grew axially along the NNE–SSW direction without shearing displacements and gas release. A field inspection by AG twice during the above period provided no evidence for elevated soil temperatures or deepening of the fissure so it is unlikely that it is related to the rearrangement of the ASTER hot-spot. Therefore the 13 June 2002 hot-spot shift is probably a result of an overpressure episode within the hydrothermal system, which is structurally controlled as Polyvotis is cut by NE–SW normal faults (figure 4; Marini *et al.* (1993)). The same episode may be also responsible for the detected high Q_{rel} for Kaminakia during the same (13 June 2002) overpass (figure 5). Recent data (Caliro *et al.* 2005, Gottsmann *et al.* 2007) indicate that the hydrothermal system is subjected to instabilities due to input from hot fluids from the deeper magmatic source or to shallow aqueous fluid migration.

4. Conclusions

1. Image analysis of ASTER night-time scenes of the Nisyros volcano suggests an almost steady state of heat flux over the period 2001–2005.

2. An average value of 36 MW (± 6 MW) of radiative heat flux is obtained inside the caldera at the time of ASTER overpass. This value is the 'background' reference heat flux for this volcano.
3. Heat-flux estimates are highly sensitive to water vapour pressure, so radiosonde data from launches closer to this volcano would provide more accurate results.

Finally, the present study also confirms that the use of information from multispectral infrared sensors orbiting from space, such as ASTER, offers a very promising method for the estimation of geophysical variables that are related to the monitoring of hydrothermal volcanic activity. Radiative heat flux is of key interest as this is often an important indicator of the complex processes underlying the event of a possible eruptive condition. The present study comprises the first comprehensive attempt to invert for this important feature using ASTER satellite data in the Nisyros volcano, one of the many hydrothermally active volcanoes in the Mediterranean.

Acknowledgements

This research was funded by the GEOWARN project (IST-1999-12310), The National Observatory of Athens and the General Secretariat for Research and Technology of Greece. GP was funded by the State Scholarships Foundation of Greece (IKY). We thank our colleagues V. Dietrich, S. Vassilopoulou, V. Sakkas, G. Vougioukalakis, G. Chiodini, K. Haritos and G. Stavrakakis for their comments and field assistance. We also thank two anonymous reviewers and the journal editor for comments and suggestions. We are indebted to the people of the Nisyros Municipality for their help. The meteorological data were retrieved from http://weather.uwyo.edu/upperair/sounding.html

References

Abrams, M. and Hook, S., 1999, ASTER user handbook. Jet Propulsion Laboratory and EROS data centre, pp 135. Available online at: http://asterweb.jpl.nasa.gov/content/03_data/04_Documents/aster_user_guide_v2.pdf (accessed 14 April 2007).

Aster Science Project User's Guide, 2005, Geolocation error of ASTER data in the longitude direction and its correction. Available online at: http://www.science.aster.ersdac.or.jp/en/documnts/users_guide/part2/07_03.html (accessed 14 April 2007).

Bonneville, A., Vasseur, G. and Kerr, Y., 1985, Satellite thermal infrared observations of Mt. Etna after the 17 March 1981 eruption. *Journal of Volcanology Geothermal Research*, **24**, pp. 293–313.

Caliro, S., Chiodini, G., Galluzzo, D., Granieri, D., La Rocca, M., Saccorotti, G. and Ventura, G., 2005, Recent activity of Nisyros volcano (Greece) inferred from structural, geochemical and seismological data. *Bulletin of Volcanology*, **67**, pp. 358–369.

Chiodini, G., Brombach, T., Caliro, S., Cardellini, C., Marini, L. and Dietrich V., 2002, Geochemical indicators of possible ongoing volcanic unrest at Nisyros Island (Greece). *Geophysical Research Letters*, **29**, 1759, doi:10.1029/2001GL014355.

Coolbaugh, M.F., Kratt, C., Fallacaro, A., Calvin, W.M. and Taranik, J.V., 2007, Detection of geothermal anomalies using Advanced Spaceborne Thermal Emission and Reflection Radiometer (ASTER) thermal infrared images at Bradys Hot Springs, Nevada, USA. *Remote Sensing of Environment*, **106**, pp. 350–359.

Fujisada, H., Sakuma, F., Ono, A. and Kudoh, M., 1998, Design and preflight performance of ASTER instrument protoflight model. *IEEE Transactions Geosciences Remote Sensing*, **36**, pp. 1152–1160.

Ganas, A. and Lagios, E., 2003, LANDSAT 7 thermal imaging of the Nisyros Volcano. *International Journal of Remote Sensing*, **24**, pp. 1579–1586.

Ganas, A., Vassilopoulou, S., Lagios, E., and Sakkas, V., 2003, Thermal imaging of Nisyros Volcano (Aegean Sea) using ASTER data. *Bulletin of the Geological Society of Greece*, **35**, pp. 108–117.

Gaonac'h, H., Vandemeulebrouck, J., Stix, J. and Halbwachs, M., 1994, Thermal infrared satellite measurements of volcanic activity at Stromboli and Vulcano. *Journal of Geophysical Research*, **99**, pp. 9477–9485.

Georgalas, G.C., 1962, *Catalogue of the Active Volcanoes of the World Including Solfatara Fields; Part XII Greece* (Rome: International Association of Volcanology).

Gillespie, A., Cothern, J.S., Rokugawa, S., Matsunaga, T., Hook, S.J. and Kahle, A.B., 1998, A temperature and emissivity separation algorithm for Advanced Spaceborne Thermal Emission and Reflection Radiometer (ASTER) images. *IEEE Transactions on Geosciences and Remote Sensing*, **36**, pp. 1113–1126.

Gogu, R.C., Dietrich, V.J., Jenny, B., Schwandner, F.M., and Hurni, L., 2006, A geo-spatial data management system for potentially achive volcanoes – GEOWARN project. *Computers & Geosciences*, **32**, pp. 29–41.

Gottsmann, J., Carniel, R., Coppo, N., Wooller, L., Hautmann, S. and Rymer, H. 2007, Oscillations in hydrothermal systems as a source of periodic unrest at caldera volcanoes: Multiparameter insights from Nisyros, Greece. *Geophysical Research Letters*, **34**, L07307, doi:10.1029/2007GL029594.

Harris, A.J.L. and Stevenson, D.S., 1997, Thermal observations of degassing open conduits and fumaroles at Stromboli and Vulcano using remotely sensed data. *Journal of Volcanology and Geothermal Research*, **76**, pp. 175–198.

Hyland, R.W. and Wexler, A., 1983, Formulations for the thermodynamic properties of the saturated phases of H2O from 173.15 K to 473.15 K. *ASHRAE Transactions*, **89**, pp. 500–519.

Lagios, E., Sakkas, V., Parcharidis, I.S. and Dietrich, V., 2005, Ground deformation of Nisyros Volcano (Greece) for the period 1995–2002: Results from DInSAR and DGPS observations. *Bulletin Volcanology*, **68**, pp. 201–214.

Lagios, E., Vassilopoulou, S., Sakkas, V., Dietrich, V., Damiata, B.N. and Ganas, A., 2007, Testing satellite and ground thermal imaging of low-temperature fumarolic fields: The dormant Nisyros Volcano (Greece). *ISPRS Journal of Photogrammetry and Remote Sensing*, **62**, pp. 447–460.

Marini, L., Principe, C., Chiodini, G., Cioni, R., Fytikas, M. and Marinelli, G., 1993, Hydrothermal eruptions of Nisyros (Dodecanese, Greece). Past events and present hazard. *Journal Volcanology Geothermal Research*, **56**, pp. 71–95.

Oppenheimer, C., 1991, Lava flow cooling estimated from Landsat Thematic Mapper infrared data: the Lonquimay eruption (Chile, 1989). *Journal of Geophysical Research*, **96**, pp. 21865–21878.

Papadopoulos, G.A., Sachpazi, M., Panopoulou, G. and Stavrakakis, G., 1998, The volcanoseismic crisis of 1996–97 in Nisyros, SE Aegean Sea, Greece. *Terra Nova*, **10**, pp. 151–154.

Pieri, D. and Abrams, M., 2004, ASTER watches the world's volcanoes: a new paradigm for volcanological observations from orbit. *Journal of Volcanology and Geothermal Research*, **135**, pp. 13–28.

Pieri, D. and Abrams, M., 2005, ASTER observations of thermal anomalies preceding the April 2003 eruption of Chikurachki volcano, Kurile Islands, Russia. *Remote Sensing of Environment*, **99**, pp. 84–94.

Ramsey, M. and Dehn, J., 2004, Spaceborne observations of the 2000 Bezymianny, Kamchatka eruption: the integration of high-resolution ASTER data into near real-time monitoring using AVHRR. *Journal of Volcanology and Geothermal Research*, **135**, pp. 127–146.

Rothery, D.A., Francis, P.W. and Wood, C.A., 1988, Volcano monitoring using short wavelength infrared data from satellites. *Journal of Geophysical Research*, **93**, 7993–8008.

Sachpazi, M., Kontoes, C.H., Voulgaris, N., Laigle, M, Vougioukalakis, G., Sykioti, O., Stavrakakis, G., Baskoutas, J., Kalogeras, J. and Lepine, J.C.L., 2002, Seismological and SAR signature of unrest at Nisyros caldera, Greece. *Journal of Volcanology and Geothermal Research*, **116**, pp. 19–33.

Sykioti, O., Kontoes, C.C., Elias, P., Briole, P., Sachpazi, M., Paradissis, D. and Kotsis, I., 2003, Ground deformation at Nisyros volcano (Greece) detected by ERS-2 SAR differential interferometry. *International Journal of Remote Sensing*, **24**, pp. 183–188.

Teschner, M., Faber, E., Poggenburg, J., Vougioukalakis, G.E. and Hatziyannis, G., 2007, Continuous, direct gas-geochemical monitoring in hydrothermal vents: Installation and long-term operation on Nisyros Island (Greece). *Pure and Applied Geophysics*, **164**, pp. 2549–2571.

Vaughan, R.G. and Hook, S.J., 2006, Using satellite data to characterize the temporal thermal behavior of an active volcano: Mount St. Helens, WA. *Geophysical Research Letters*, **33**, L20303, doi:10.1029/2006GL027957.

Vougioukalakis, G., 1993, Volcanic stratigraphy and evolution of Nisyros Island. *Bulletin of the Geological Society of Greece*, **28**, pp. 239–258.

Yamaguchi, Y., Fujisada, H., Kudoh, M., Kawasaki, T., Tsu, H., Kahle, A.B. and Pniel, M., 1999, ASTER instrument characterization and operation scenario. *Advances in Space Research*, **23**, pp. 1415–1424.